ACCURATE MEASUREMENT OF THREE-DIMENSIONAL NATURAL KNEE KINEMATICS USING SINGLE-PLANE FLUOROSCOPY

By

HASEEB AHMAD RAHMAN

A THESIS PRESENTED TO THE GRADUATE SCHOOL
OF THE UNIVERSITY OF FLORIDA IN PARTIAL FULFILLMENT
OF THE REQUIREMENTS FOR THE DEGREE OF
MASTER OF SCIENCE

UNIVERSITY OF FLORIDA

2004

ACKNOWLEDGMENTS

I would like to thank everyone who has supported me in my project. And I know that although some people use the acknowledgements section to include fellows who have very little to do with the actual project but who are part of their support system, “a shout out to the homies,” if you will, I will try to keep it short. Therefore, I would like to impart these words of wisdom that I have picked up along the way, and that have probably saved my sanity more times than I can remember.

Above all, I would like to thank my family without whom I would never have even started, especially my sister, who was always there to distract or direct me, although I am not sure she always did it at the right times.

I would also like the people that I worked with on a daily basis to know that in a strange way, they have grown on me. So, hopefully we will keep in touch. But do know that I really did appreciate everything that you have done for me, whether it be a reassuring “Don’t worry, you’ll graduate,” or just discussing the politiks of the different countries of the world. Hey it was fun while it lasted.

TABLE OF CONTENTS

Page

LIST OF TABLES

LIST OF FIGURES

Abstract of Thesis Presented to the Graduate School
of the University of Florida in Partial Fulfillment of the
Requirements for the Degree of Master of Science

ACCURATE MEASUREMENT OF THREE-DIMENSIONAL NATURAL KNEE KINEMATICS USING SINGLE-PLANE FLUOROSCOPY

By

Haseeb Ahmad Rahman

August 2004

Chair: Benjamin J. Fregly
Major Department: Biomedical Engineering

An understanding of the relationship between knee joint kinematics and injury or disease (e.g., osteoarthritis) can be best achieved by studying the joint under *in vivo*, dynamic, and loaded conditions. While bone models matched to single-plane fluoroscopic images have recently been employed to measure three-dimensional natural knee kinematics under such conditions, the accuracy of this procedure has not been well quantified. This study used a three-step computational approach to address this issue. First, subject-specific bone models of the femur, tibia/fibula, and patella were created from CT scan data. Next, synthetic fluoroscopic images were generated with the bone models in known random poses (i.e., translations and rotations). Finally, an automated matching procedure using iterative unidirectional optimization with cubic curve fitting was developed to align the edge-detected bone models to the synthetic images. When flat-shading was used to generate images with sharp edges, little to no bias was present in the measured absolute pose parameters. The precision for the femur and tibia/fibula was

less than 0.2 mm for in-plane translations and 0.5° for all rotations while for the patella it was less than 0.4 mm for in-plane translations and 2° for all rotations. When ray-tracing was used to generate more realistic images with attenuated edges, measurement bias appeared and precision decreased by a factor of two for the femur and tibia/fibula and two to four for the patella. When relative pose parameters were calculated for the ray-traced images, the precision for tibiofemoral kinematics was about 2 mm for in-plane translations and 1° for all rotations, while for patellofemoral kinematics it was about 4 mm for in-plane translations, 1° for in-plane rotation, and 5° for out-of-plane rotations. The proposed optimization procedure is a viable option for automated image matching, though poor image edge detection resulting in systematic out-of-plane translation errors limits the accuracy of the current procedure.

CHAPTER 1
BACKGROUND

Between 1997 and 2002, the number of Americans afflicted with arthritis has more than doubled to 70 million, making arthritis the leading cause of work disability [1,2]. According to the Arthritis Foundation, the most common form of arthritis, osteoarthritis (OA), appears in the knee more than any other joint. Disease development and progression are influenced by abnormal joint kinematics under dynamic, weight-bearing conditions [3,4]. Therefore, knowledge of kinematics in healthy and arthritic knees would be extremely valuable for understanding the disease's etiology and predisposing factors as well as for guiding surgical planning, technique, and procedure.

Unfortunately, few studies have measured three-dimensional (3D) knee kinematics under loaded, physiological conditions with the accuracy needed to study arthritis-related issues. Video-based motion analysis with surface markers has been used widely to study gross body motion but less to study detailed joint motion due to the problem of skin and soft tissue motion artifacts [5-14]. Use of redundant surface markers to correct for motion artifacts shows promise and evaluation of these methods is ongoing [12,14]. However, the most direct way to eliminate these issues is to measure joint motion using x-ray techniques. For artificial knees, single-plane fluoroscopy has been used to measure implant motion directly [15-19]. With this approach, 3D static computer aided design (CAD) models of the metallic components are aligned to each 2D dynamic fluoroscopic image to quantify pose (translation and rotation) parameters. For natural knees, since CAD models of the bones are not readily available from the manufacturer, bi-plane

fluoroscopy with implanted bone markers has been used instead [20-22]. Though more accurate than single-plane fluoroscopy, this approach requires a more complex and costly experimental set-up and is mildly invasive due to implantation of tantalum beads.

Building on artificial knee studies, researchers have recently begun to use single-plane fluoroscopy to measure natural knee motion [23-24]. For the image matching procedure, implant CAD models are replaced with geometric bone models created from medical imaging data. However, in fluoroscopic images, cortical bone edges are less well defined than are metallic implant edges. Consequently, to determine when this approach can be used to address arthritis-related research questions, evaluation of measured bone (absolute) and joint (relative) kinematics is needed.

The purpose of this study is to quantify the absolute and relative bias and precision with which natural knee kinematics can be measured using single-plane fluoroscopy and edge-detected bone models. The four specific goals were the following: 1) to generate synthetic fluoroscopic images using bone models in known poses, 2) to develop an automated matching procedure that finds absolute and relative bone model pose parameters consistent with the synthetic images, 3) to evaluate the automated matching procedure under conditions in which bone edge definition in images is not a significant source of error, and 4) to assess the extent to which bone edge attenuation in images degrades the precision of the measurement. The results can be used to define where this measurement procedure lies in the spectrum from video-based motion analysis with surface markers to bi-plane fluoroscopy with bone markers.

CHAPTER 2
METHODS

A three-step computational approach was used to quantify the accuracy with which edge-detected bone models can be matched to single-plane fluoroscopic images of the knee. First, subject-specific bone models were created from CT scan data. Next, synthetic fluoroscopic images were generated with the bone models in known poses. Finally, an automated matching procedure was developed to align the bone models to the synthetic images. Though the methodology described here is tailored to assessment of absolute and relative measurement accuracy, it can be used equally well to measure *in vivo* bone motion from fluoroscopic images.

Bone Model Creation

Subject-specific geometric models of the femur, tibia/fibula, and patella were created from CT scan data for subsequent synthetic image generation and automated image matching. One healthy subject gave informed consent to undergo fine and coarse axial CT scans of the left leg as approved by the institutional review board. Both scans used a 512 x 512 image matrix (Fig. 1a). The fine scan used 1 mm slices spanning approximately 75 mm above and below the joint line of the knee, while the coarse scan used 5 mm slices from the hip center to the ankle center. This approach minimized radiation exposure to the subject while obtaining accurate geometric information in the knee region [23]. Interior and exterior cortical bone edges for the femur, tibia, fibula, and patella were segmented using a commercial watershed algorithm (SliceOmatic, Tomovision, Montreal, CA) (Figs. 1b and 1c). The segmentation process was semi-

automatic, requiring user intervention only for slices near the ends of the bones where volume averaging effects make edge detection more difficult. Pixels tagged by the watershed algorithm (Fig. 1a) were automatically converted to polygonal surface models using a “Connecting Cubes” algorithm [25] similar to “Marching Cubes” [26].

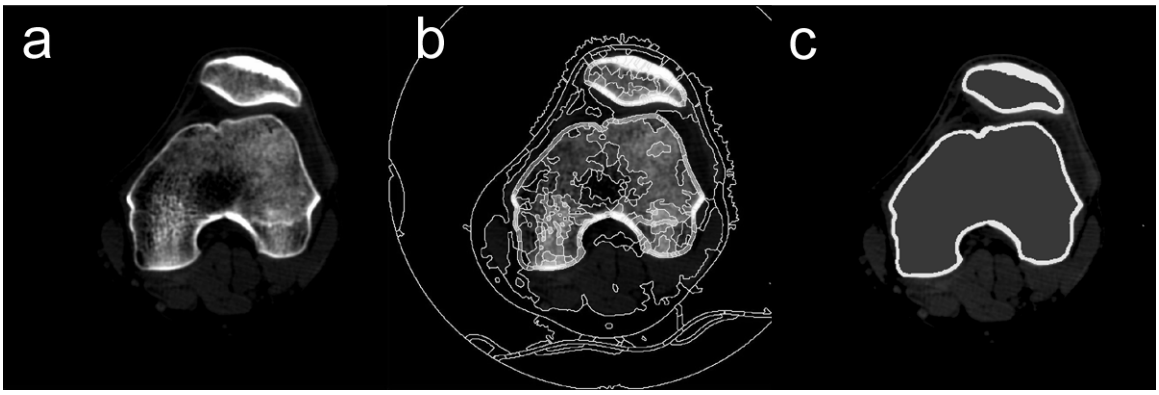

Fig 1. Watershed Algorithm of CT scan and subsequent tagging. a) Axial CT slice of femur and patella. b) CT slice with puzzle pieces derived from watershed algorithm. c) Segmented CT slice with cortical bone shown as white and cancellous bone as black.

The fine and coarse polygonal surface models were refined and combined into single cortical bone models using commercial reverse engineering software (Geomagic Studio, Raindrop Geomagic, Research Triangle Park, NC). Unrealistic flat regions in each polygonal model were deleted one at a time and the resulting holes filled automatically (Fig. 2a). The coarse polygonal models were then aligned to their fine counterparts, with the exterior and interior cortical models being aligned separately. This was achieved using an automatic three-dimensional alignment algorithm that minimized the sum of the distances between corresponding polygons in the fine scan region. The alignment was performed only for the femur and tibia/fibula. For the patella, the fine model was used directly. Coarse model polygons in the fine scan region were deleted and the gap between fine and coarse models for each bone filled automatically. To create uniform polygon density, all polygons were subdivided and then decimated back to the

original number of polygons via a curvature-based algorithm (Fig. 2b). The final bone models contained the interior and exterior cortical bone surfaces (Fig. 2c). Point clouds output from the image processing software were used to quantify the tolerance of the final polygonal surfaces, which averaged 0.15 mm over all surfaces of all bones with a standard deviation of 0.12 mm.

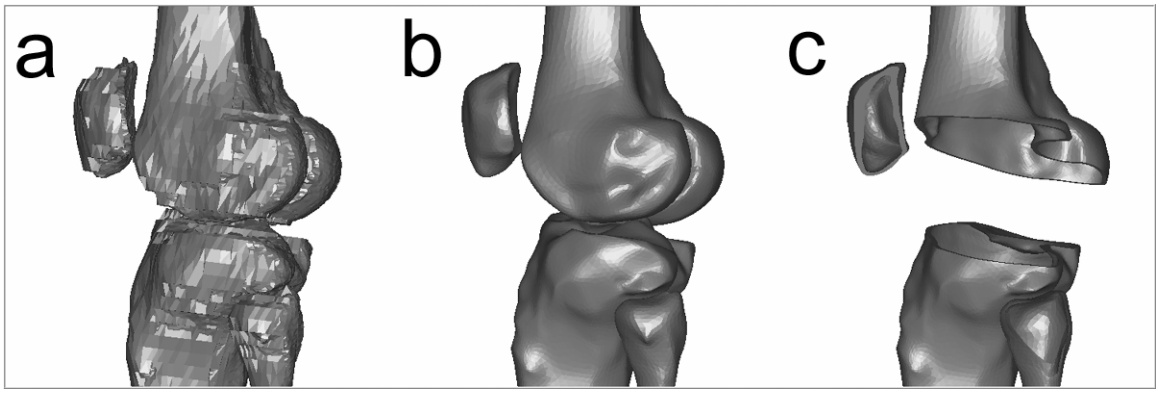

Fig 2. Series describing bone model creation process. a) Unaligned coarse and fine polygons displaying unrealistic “stair-rise” effects. b) Aligned and refined polygonal models. c) Sectioned polygon models to display inner geometry.

In preparation for fluoroscopic image matching, anatomic coordinate systems were created in each bone model [27]. The mechanical axis of the leg, as determined from CT slices through the hip and ankle centers, was used to define the superior-inferior axis for the femur and the tibia/fibula. The medial-lateral axis of the femur was defined from the transepicondylar axis, while the anterior-posterior axis of the tibia/fibula was defined by a line through the medial third of the tibial tubercle and the center of the tibial plateau. The third axis was formed from the cross product of the first two. The coordinate system origin of the femur was defined as the midpoint of the transepicondylar line, while the origin of the tibia/fibula was defined as the centroid of the tibial plateau located at the level of the articular surfaces. The patella coordinate system was identical to that of the tibia/fibula with the knee as scanned in full extension. Relative translation and rotation

between the tibia and fibula were assumed to be negligible, and the two models were combined into one for image matching purposes [24].

Synthetic Image Creation

Once the bone models were developed, synthetic images were generated to quantify the absolute and relative errors in matching these models to single-plane fluoroscopic images. Three sets of synthetic image sequences were analyzed with the bone models in known poses: 1) flat-shaded images where the three bone models were randomly transformed as a single rigid body, 2) ray traced images identical to the first sequence, and 3) ray-traced images that replicated an *in vivo* stair rise motion. Similar to the experimental conditions for the third sequence, approximately 30 synthetic images were generated for each of the three sequences.

The first synthetic image sequence used flat shading to evaluate absolute and relative measurement errors for a series of random images with the bone models in fixed relative poses. Flat shading eliminates bone edge attenuation visible in both synthetic ray-traced and experimental images. A single experimental image from the third sequence (see below) was used to define realistic absolute and relative pose parameters for the three bone models (Fig. 3a). Random transformations were then applied to the three bone models treated as a single rigid body. This assured that the relative poses of the bones would be the same in all random images. The magnitudes of the uniformly-distributed random transformations were ± 50 mm for all three translations, ± 15° for the *x* and *y* (out-of-plane) rotations, and ± 45° for the *z* (in-plane) rotation. The transformation parameters were used to position the bone models for synthetic image generation. This was achieved using commercial surface modeling and rendering software (Rhinoceros and Flamingo, Robert McNeel & Associates, Seattle, WA). The viewing properties were

configured to produce a principal distance and image scale similar to the experimental setup (see discussion), while the bone models were given light attenuating material properties similar to x-rays. Once the three bones models were placed in the desired pose, flat shading was used to generate a synthetic fluoroscopic image (Fig 3b).

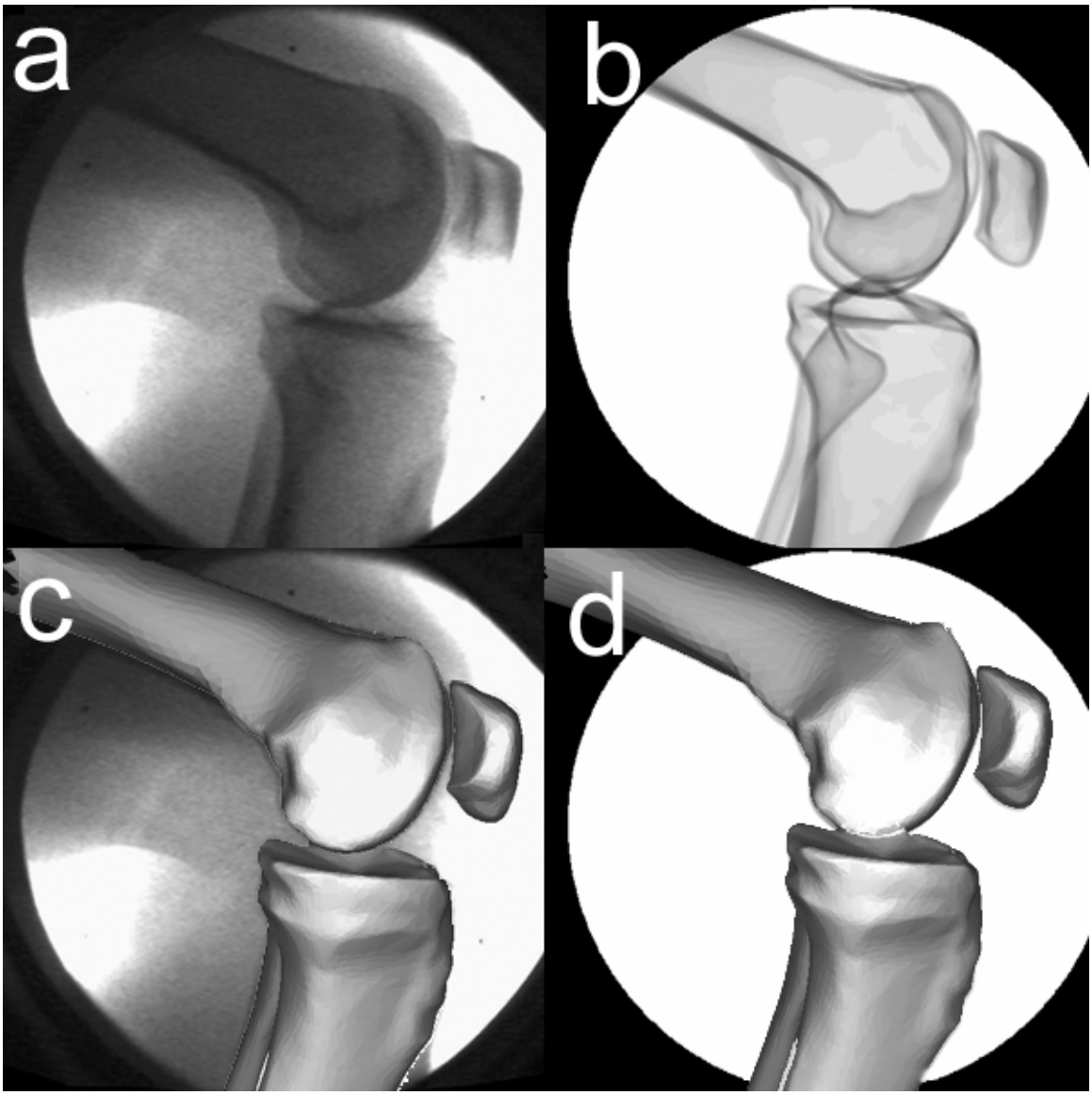

Fig 3. Images depicting synthetic image matching procedure. a) Actual fluoroscopic image of subject performing a stair maneuver. b) Synthetic image replicating stair maneuver. c) CAD model matched to fluoroscopic image. d) CAD model matched to artificial image.

This process was repeated for each pose and the resulting synthetic images output to the image matching software. The automated matching procedure (see below) was then used to align the bone models to the synthetic images and quantify the absolute and relative errors in the pose parameters. The bone models were manually placed close to their perceived best poses prior to automated matching of each image since random transformations do not produce images with pose parameter continuity [15]. Rotations were calculated using the Grood and Suntay [28] convention.

The second synthetic image sequence was identical to the first except that ray tracing was used instead of flat shading to emulate experimental images (Fig. 3c). This sequence was included to evaluate the extent to which bone edge attenuation affects the automated image matching process. All other image creation and matching steps were the same as for the first sequence.

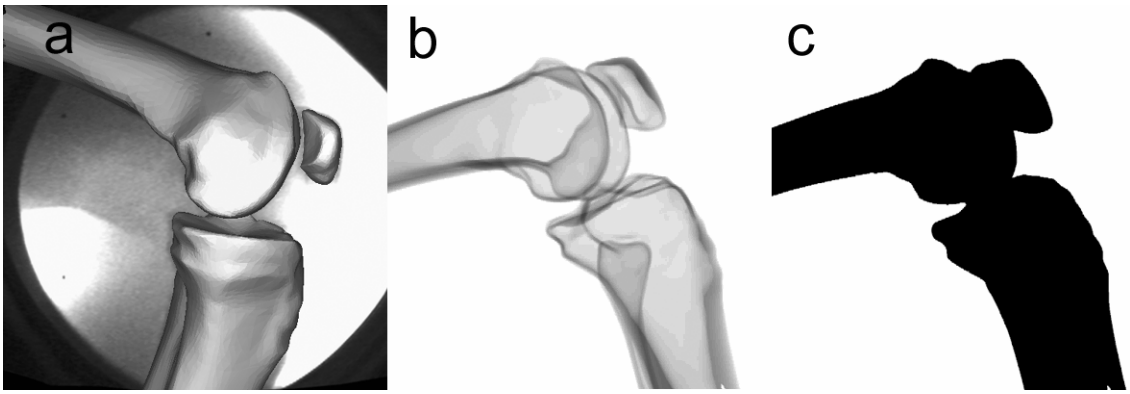

Fig 4. Synthetic x-rays. a) Knee joint positioned in a natural pose to 60º. b) Synthetic image generated with ray tracing after application of a random transform to the natural pose. c) Synthetic image generated with flat shading after application of the same random transform.

The third synthetic image sequence employed ray tracing to evaluate absolute measurement errors under loaded physiological conditions. This sequence was chosen to emulate *in vivo* testing conditions as closely as possible [21]. The same subject who provided the CT scan data gave informed consent to perform a stair rise activity under

fluoroscopic analysis using a protocol approved by the institutional review board (Fig 4a). Images were collected at 30 frames/sec producing approximately 30 frames for each of three trials. Bone models of the femur, tibia/fibula, and patella were manually aligned to the fluoroscopic images from one of the trials using custom software (Fig. 4b) [16,29]. Using the manually determined poses, the synthetic image creation process (Fig. 4c) and subsequent automated image matching procedure (Fig. 4d) noted above were repeated. Similar to the methodology for artificial knees, the pose parameters found for one frame were used as the initial guesses for the subsequent frame.

Automated Image Matching

Given the synthetic image sequences with the bones in known poses, the next step was the development of an automated image matching procedure that produced the same match regardless of the expertise of the user. For each bone, the general concept was to edge detect the bone model, then edge detect the same bone in the fluoroscopic image, and finally move the bone model until its edges best matched those in the image. Canny edge detection was used on both the bone model and the fluoroscopic image. Matching was achieved by developing a novel optimization procedure (details below) whose cost function minimized the normalized sum of the distances between the two sets of edge points. Distance was measured in units of pixels and calculated from image edges, which remain constant for a particular image, to bone edges, which change as the bone model pose is modified. Normalization based on the number of selected image edge points was performed to make the results insensitive to this variable. Interior geometric features were not detected and used in the cost function due to the high computational cost of repeatedly ray tracing each bone model. To simplify bone edge detection in each fluoroscopic image, a mask was placed around the edges of the bone model in its initial

pose, and only those image points located within the mask were used for image edge detection.

The optimization procedure was based on the Univariate Search Method (see discussion for justification), which minimizes errors in one pose parameter at a time rather than all six pose parameters simultaneously. The order in which the six pose parameters were optimized was determined by calculating the sensitivity of the cost function to changes in each pose parameter separately. The pose parameters were defined such that *x* and *y* corresponded to anterior-posterior (A-P) and superior-inferior (S-I) in-plane translations, respectively, while *z* corresponded to medial-lateral (M-L) out-of-plane translation. Varus-valgus (V-V), internal-external (I-E), and flexion-extension (F-E) rotations were calculated using the same axes. The three most sensitive directions (in-plane parameters: *x* and *y* translations and *z* rotation) were optimized first, followed by the three least sensitive directions (out-of-plane parameters: *x* and *y* rotations and *z* translation). The entire sequence of six one-dimensional optimizations was iterated until the specified absolute or relative convergence tolerance was met.

For each one-dimensional optimization, a six-step curve-fitting approach was used to find the minimum (Fig. 5; see Discussion for justification). First, seven points with wide initial spacing were sampled along the search direction (Fig. 5a). Second, these points were re-sampled so that the lowest point was in the middle, essentially shifting the sampled points in one direction or the other while maintaining the same spacing (Fig. 5b). Third, a cubic polynomial, which only requires four sampled points, was fit through the seven points using linear least squares (Fig. 5c). A cubic was chosen instead of a quadratic since the cost function was asymmetric about the minimum for each search

direction. Fourth, the redundant points were used to assess the goodness of fit of and noise present in the cubic. Goodness of fit was quantified by calculating the adjusted R^2 value, while noise was quantified by calculating the standard error of the estimate *s*. Fifth, an automatic stepsize adjustment algorithm (see below) was used to adjust the point spacing until R^2 was greater than 0.99 and *s* was less than 1. These values were chosen empirically based on experience with the algorithm. Finally, once a cubic curve fit was found meeting these two criteria, the minimum was calculated analytically (Fig. 5d).

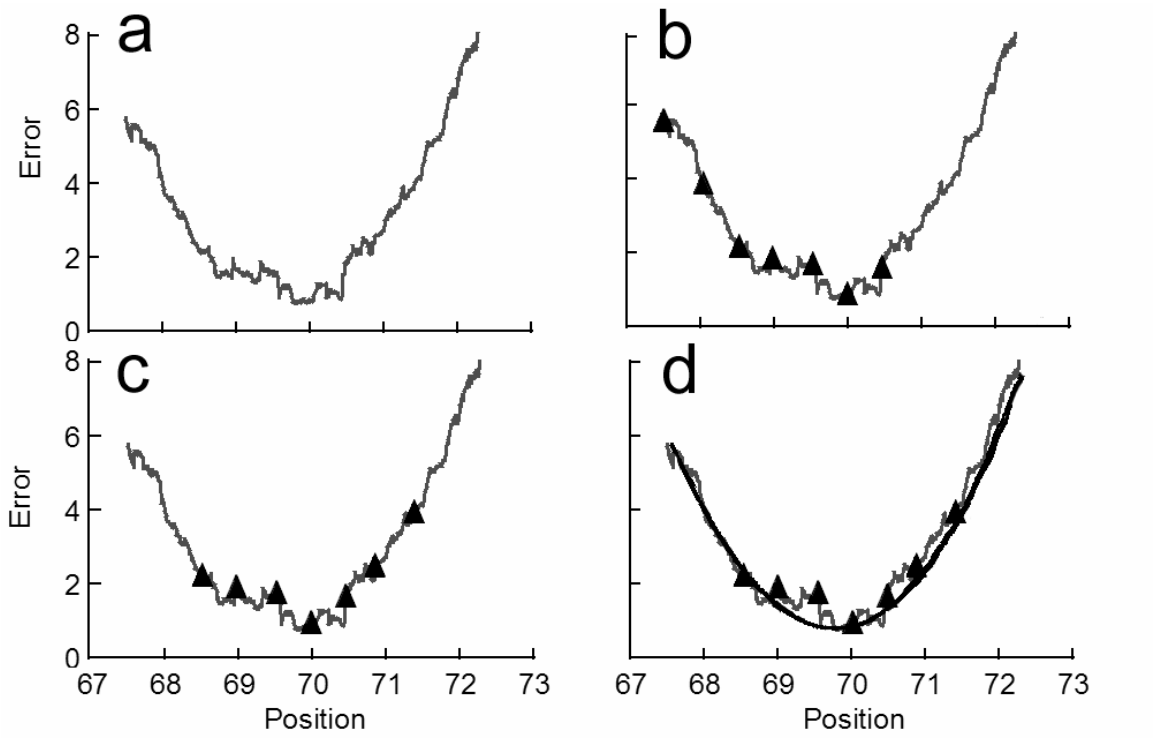

Fig 5. Univariate search steps. a) Noisy cost function of z (in-plane) rotation. b) Seven evaluations of the cost function given an initial guess of 69º and a step size of 0.5º. c) Seven evaluations re-centered to put the smallest error in the middle. d) Cubic function fit through the seven evaluations. Note that the optimal value for the frame was 70º.

Central to this approach is the automatic stepsize adjustment algorithm used to produce stable and rapid convergence. Neither R^2 nor *s* alone was sufficient to identify cubic curve fits that accurately predicted the minimum. However, when R^2 and *s*

information were combined, four separate combinations (or regions) were identified that could be used to guide the stepsize adjustment process (Fig. 6). These regions were defined as follows: Region 1 - $R^2 < 0.99$, $s < 1$; Region 2 - $R^2 > 0.99$, $s < 1$; Region 3 - $R^2 > 0.99$, $s > 1$; Region 4 - $R^2 < 0.99$, $s > 1$. The goal was to find a cubic curve fit in Region 2, where the goodness of fit was high and noise low. Once a candidate cubic fit was generated as described above, the region was identified from the fit's R^2 and s values. The step size was then adjusted based on the following general algorithm: Region 1 – Double the step size; Region 2 – Test for convergence; Region 3 – Halve the step size; Region 4 – Quarter the step size. If the fit lay in region 2 but did not pass the convergence test, the step size was halved. In addition, the previous region found was stored and used to make additional step size adjustments to avoid stepping over Region 2 in one direction or the other. This six-step process was iterated until the specified absolute or relative tolerance was met.

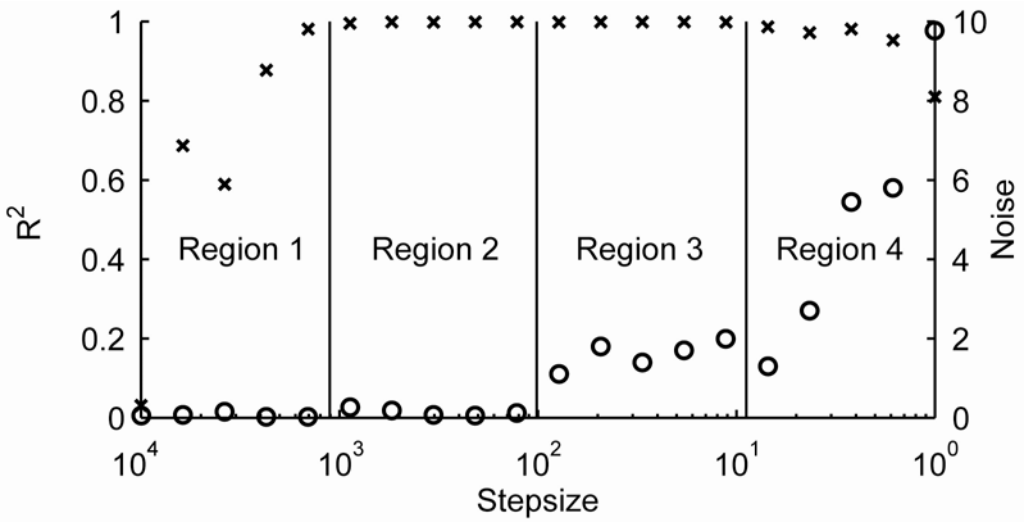

Fig 6. Stepsize regions. Region 1 - $R^2 < 0.99$, $s < 1$; Region 2 - $R^2 > 0.99$, $s < 1$; Region 3 - $R^2 > 0.99$, $s > 1$; Region 4 - $R^2 < 0.99$, $s > 1$.

Data Analysis

Similar to a recent study published by Tashman and Anderst [21], the accuracy of the automated image matching process was quantified using bias and precision. Bias was calculated from the mean matching error for each of the six pose parameters in each synthetic sequence, while precision was calculated from the corresponding standard deviations. For bias results, a Student's t-test ($p < 0.05$) was performed to determine if the values were statistically different from zero, indicating the presence of a systematic error. Bias and precision were calculated for the absolute and relative pose parameters from the first and second synthetic sequences and for only absolute pose parameters from the third synthetic sequence. The automated image matching procedure was also evaluated qualitatively for real images by comparing pose parameters determined via manual matching with those determined automatically. The experimental images used to generate the third synthetic sequence were used in this evaluation.

CHAPTER 3
RESULTS

For the synthetic flat-shaded image sequence with randomly transformed bones in a fixed relative pose, almost no statistically significant bias was present in any of the absolute pose parameters for any of the bones (Table 1). When bias was detected, it was extremely small (less than 0.08 mm and 0.05°). For the femur and tibia/fibula, the measurement precision was at least 0.20 mm for the in-plane translations and 0.14° for the in-plane rotation, while it was 0.47° for the out-of-plane rotations and 3.1 mm for the out-of-plane translation. As expected, the precision results for the patella were worse, more so for the out-of-plane than in-plane pose parameters.

When the image creation process was changed to ray tracing, measurement bias increased and precision decreased in the absolute pose parameters, with out-of-plane precision for the patella becoming much worse than for the femur or tibia/fibula (Table 2). Ten rather than three of the pose parameters demonstrated statistically significant measurement bias, with the bias being larger than in the corresponding flat-shaded sequence. For all three bones, translation bias was as large as 0.42 mm in plane and 12 mm out of plane, the latter always being in the negative z direction. Out-of-plane rotation bias was as large as 0.60° (with the exception of patella x rotation), with no in-plane rotation bias being detected. The femur and tibia/fibula precision results were approximately two times worse than for the corresponding flat shaded sequence, while for the patella they were approximately two to four times worse.

When relative pose parameters were calculated for the same two synthetic sequences, bias trends were similar to the absolute results, while precision generally decreased by more than the sum of the corresponding absolute results (Table 3). For example, anterior-posterior translation precision for the flat-shaded femur/tibia was 0.86 mm, while the sum of the *x* translation precisions for the flat-shaded femur and tibia was 0.36 mm. A small bias (< 0.06°) was detected in only one relative pose parameter for the flat-shaded sequence, while bias was detected in all but one of the relative pose parameters in the ray-traced sequence. Relative translation biases were between 0.70 and 8.2 mm, while relative rotation biases were between 0.25 and 2.2°. Changing from the flat-shaded to the ray-traced sequence decreased the precision of the relative pose parameters by a factor of two to four. Precision dropped from at least 0.86 to 3.5 mm for A-P and S-I translations, 0.20 to 0.43° for F-E, 1.8 to 5.2° for V-V and I-E rotations, and 4.0 to 10 mm for M-L translation.

The absolute pose parameter results for the synthetic ray-traced image sequence corresponding to *in vivo* experimental stair rise data were generally consistent with the results from the ray-traced random sequence (Table 4). Statistically significant bias comparable to that of the ray-traced random sequence was detected in six of the pose parameters, with *z* translation bias again being in the negative direction. Precision results were also comparable to the ray-traced random sequence for most pose parameters. The tibia/fibula was the primary exception, where the precision of many pose parameters was one and a half to three times worse. For the patella, *x* translation and *z* rotation precision were also much worse.

The qualitative evaluation with weight-bearing experimental fluoroscopic images revealed that automated image matching was consistent with manual matching performed by an experienced user. When comparing relative pose parameters (Fig. 7), the automated and manually matched curves were extremely similar. The one exception was the medial-lateral (out-of-plane) translation, where automated matching produced a smoother, more continuous curve.

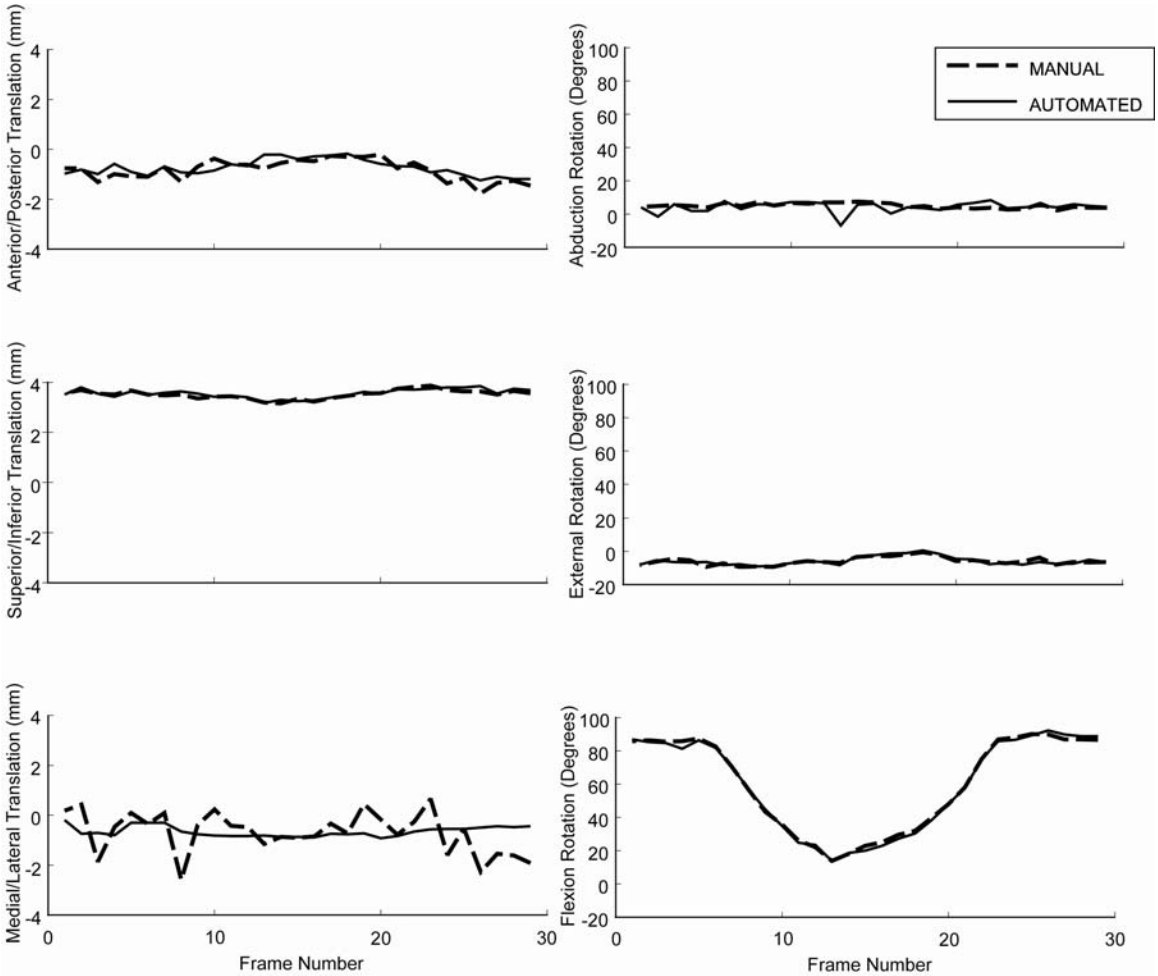

Fig 7. Qualitative comparison between manual and automated matched relative kinematics of an *in vivo* image set.

Table 1. Absolute pose parameter bias ± precision calculated from three synthetic flat-shaded and ray-traced image sets corresponding to randomly transformed bones in a fixed relative pose or an *in vivo* experimental stair rise motion.

Synthetic Images	Pose Parameters	Femur	Tibia/Fibula	Patella
Set 1 Flat-Shaded Random	X translation (mm)	0.037 ± 0.16	-0.037 ± 0.20	0.078 ± 0.11*
	Y translation (mm)	-0.058 ± 0.13*	0.0093 ± 0.18	-0.021 ± 0.34
	Z translation (mm)	0.57 ± 2.3	-0.46 ± 3.1	0.22 ± 4.2
	X rotation (deg)	-0.14 ± 0.47	0.028 ± 0.45	-0.39 ± 1.3
	Y rotation (deg)	0.060 ± 0.29	-0.074 ± 0.29	0.25 ± 1.7
	Z rotation (deg)	-0.046 ± 0.093*	-0.0012 ± 0.14	0.0064 ± 0.18
Set 2 Ray-Traced Random	X translation (mm)	0.17 ± 0.28*	0.31 ± 0.37	0.41 ± 0.30*
	Y translation (mm)	0.059 ± 0.20	-0.42 ± 0.36*	-0.044 ± 0.43
	Z translation (mm)	-6.7 ± 5.7*	-11 ± 7.6*	-12 ± 10*
	X rotation (deg)	-0.32 ± 0.65*	-0.043 ± 0.87	-2.9 ± 5.3*
	Y rotation (deg)	0.56 ± 0.60*	-0.14 ± 0.65	0.60 ± 1.7*
	Z rotation (deg)	-0.19 ± 0.36	0.014 ± 0.34	-0.021 ± 0.10
Set 3 Ray-Traced Experimental	X translation (mm)	-0.031 ± 0.27	-0.12 ± 1.2	0.25 ± 1.0
	Y translation (mm)	0.043 ± 0.28	-0.24 ± 0.43*	-0.024 ± 0.32
	Z translation (mm)	-3.3 ± 5.6*	-10 ± 7.2*	0.70 ± 9.7
	X rotation (deg)	0.15 ± 0.47	-0.21 ± 2.1	-6.5 ± 3.7*
	Y rotation (deg)	0.99 ± 0.72*	0.17 ± 1.1	2.2 ± 2.3*
	Z rotation (deg)	-0.028 ± 0.56	0.22 ± 0.68*	-0.25 ± 1.1

* indicates bias is statistically different from zero ($p < 0.05$) based on a Student's t-test

Table 2. Relative pose parameter bias ± precision calculated from three synthetic flat-shaded and ray-traced image sets corresponding to randomly transformed bones in a fixed relative pose or an *in vivo* experimental stair rise motion.

Synthetic Images	Pose Parameters	Tibiofemoral	Patellofemoral
Set 1 Flat-Shaded Random	A-P translation (mm)	0.26 ± 0.86	0.070 ± 0.62
	S-I translation (mm)	-0.014 ± 0.85	-0.14 ± 0.55
	M-L translation (mm)	0.50 ± 3.93	0.75 ± 4.0
	V-V rotation (deg)	0.065 ± 0.62	-0.28 ± 1.3
	I-E rotation (deg)	0.098 ± 0.50	0.37 ± 1.8
	F-E rotation (deg)	-0.058 ± 0.18*	-0.058 ± 0.20
Set 2 Ray-Traced Random	A-P translation (mm)	1.0 ± 2.1*	1.6 ± 3.5*
	S-I translation (mm)	1.1 ± 1.9*	0.70 ± 1.9*
	M-L translation (mm)	3.0 ± 8.1*	8.2 ± 10*
	V-V rotation (deg)	0.53 ± 1.1*	-2.2 ± 5.2*
	I-E rotation (deg)	0.22 ± 0.93	0.62 ± 1.7*
	F-E rotation (deg)	-0.25 ± 0.39*	-0.32 ± 0.43*
Set 3 Ray-Traced Experimental	A-P translation (mm)	3.1 ± 4.7*	-0.087 ± 2.5
	S-I translation (mm)	0.89 ± 0.91*	0.82 ± 1.9*
	M-L translation (mm)	10 ± 14*	0.56 ± 11
	V-V rotation (deg)	0.34 ± 2.2	-4.9 ± 4.6*
	I-E rotation (deg)	-0.51 ± 1.6*	0.94 ± 2.0*
	F-E rotation (deg)	-0.33 ± 0.73*	-0.44 ± 0.97*

* indicates bias is statistically different from zero ($p < 0.05$) based on a Student's t-test

Table 3. Comparison of pose parameter precision from the present study with knee x-ray studies in the literature.

Reference	Fluoroscopy Method	Models Matched	Knee Type	Kinematics	In-Plane Translation(mm)	Out-of-Plane Translation(mm)	Rotation (deg)
Present study	Single-plane	Bones	Natural	Absolute	0.68	2.7	0.28
Present study	Single-plane	Bones	Natural	Relative	0.86	3.9	0.86
Banks and Hodge [23]	Single-plane	Implants	Artificial	Absolute	0.48	6.6	1.1
Banks and Hodge [23]	Single-plane	Implants	Artificial	Relative	0.17	3.9	1.2
Kanisawa *et al*. [22]	Single-plane	Bones	Natural	Absolute	1.2	4.0	0.8
Komistek *et al*. [21]	Single-plane	Bones	Natural	Absolute	0.45	Not reported	0.66
Tashman *et al*. [19,20]	Bi-plane	Beads	Natural	Absolute	0.14	0.14	1.0
Kaptein *et al*. [13]	Bi-plane	Implants	Artificial	Absolute	0.06	0.14	0.1
Zollei *et al*. [14]	Single-plane	Bones	Natural	Absolute	0.82	??	0.11

CHAPTER 4
DISCUSSION

This study used a computational approach to quantify the accuracy with which natural knee kinematics can be measured using single-plane fluoroscopy and edge detected bone models. Three-dimensional bone models were created from CT scan data and used for generating synthetic fluoroscopic images. Accuracy was assessed in terms of bias and precision. Recovery of pose parameters with little to no measurement bias for the flat-shaded image sequence indicates that the proposed automated image matching procedure works properly. The appearance of measurement bias and decrease in measurement precision when ray tracing was used instead of flat shading indicates that bone edge attenuation is a significant confounding factor. Furthermore, the worse-than-expected precision results for the relative compared to absolute pose parameters when little bias was present indicates coupling between the absolute parameter errors. Based on the random and experimental ray-traced synthetic sequences, we estimate that the measurement precision for tibiofemoral kinematics is about 2 mm for in-plane translations and 1° for all rotations, while for patellofemoral kinematics it is about 4 mm for in-plane translations, 1° for in-plane rotation, and 5° for out-of-plane rotations. For both joints, the precision for out-of-plane translation is about 10 mm.

A computational rather than experimental approach was used in this study to provide a well-controlled environment for determining accuracy. If the accuracy determined by this method was poor given a specific desired application, little motivation

would exist for a corresponding experimental evaluation. Similar errors for the synthetic random and experimental sequences suggest that the random results were representative of *in vivo* conditions. Thus, our results can be used to infer the approximate accuracy that could be obtained from single-plane fluoroscopic images with clear though attenuated bone edges.

The results from the three synthetic sequences were consistent with an intuitive understanding of the process and previous research. For absolute pose parameters, the in-plane translations (x, y) and rotation (z) were matched more accurately than were the out-of-plane translation (z) and rotations (x, y) (Tables 1, 2, and 4). These findings were consistent with the preliminary sensitivity study on which the optimization methodology was based and with previous single-plane fluoroscopic studies of artificial knees [17,18]. Also, absolute precision results were generally related to the amount of distinguishing bone geometry present, with the patella being matched less precisely than the femur or tibia/fibula. What was encouraging, however, was that the patella could be matched at all, allowing reasonably accurate quantification (less than about 4 mm and 1°) of in-plane patellofemoral kinematics.

The accuracy results for the reported technique are similar to the results for other techniques (Table 3). When using the automated matching procedure to match single-plane flat-shaded images and bone models pose precisions were on the same magnitude of single-plane fluoroscopy and implant models. This is expected since fluoroscopic images of implants show clear and definite edges similar to synthetic images using flat-shading. Using this technique rotational precision was found to be more accurate than most techniques. Although bi-planar fluoroscopy using implant models produces greater

precision, it requires tantalum bead implants and two fluoroscopic cameras. For this study, out-of-plane translation precisions were larger than in-plane. This result was similar to other studies using single-plane fluoroscopy. Relative precision errors were comparable to absolute precision errors, as seen in other studies.

Higher-level optimization methods were not chosen for reasons specific to our study. Global optimization would have required excessive CPU time due to the large number of costly function evaluations. Gradient-based optimization [16] was implemented but not chosen due to a discontinuous cost function in each direction (Fig. 5a). As the bone model pose was modified during gradient calculations, image edge points were compared with different bone model edge points, producing inaccurate search directions. This caused convergence to a local minimum or overshooting of the true minimum, depending on the current step size. Response surface methods fitting more than one pose parameter at a time were also unsuccessful due to the noisy nature of the search space.

The relative precision results revealed that coupling existed between the absolute pose parameter errors. For the flat-shaded random results, one might expect the precision of the relative pose parameters to be no worse than the sum of the corresponding absolute precisions, since little bias was present. However, this was not the case for except for medial-lateral translation. After a random transform was applied to the three bones as a single rigid body, the relative kinematic directions were no longer aligned with the absolute kinematic directions. For example, if a 90° *y* axis rotation had been applied to the three bones, anterior-posterior translation would now be measured in the *z* direction, which is the least precise, while medial-lateral translation would now be measured in the

x direction. Thus, absolute measurement errors from multiple directions appear in the relative precision results. Since 15° would be a large *y* rotation misalignment under experimental conditions, the relative precision results reported here likely represent an upper bound on the *in vivo* situation for the knee.

Poor image edge detection resulting in systematic *z* translation errors appears to be the primary source of error in the analysis. The fact that large *z* translation bias did not exist in the flat-shaded synthetic images indicates that it was due to bone edge attenuation in the ray-traced synthetic images. Since this bias was consistently in the negative *z* direction, the automated image matching procedure was pushing the bone models backward to shrink their edges inward and match the attenuated edges of the bone models. This systematic adjustment likely introduced the bias present in the other absolute pose parameters (Table 2). Furthermore, the random transforms applied to the three bones simultaneously may have propagated this bias to nearly all of the relative pose parameters in the ray-traced synthetic images (Table 3). These effects also resulted in worse relative precision for the ray-traced compared to flat-shaded images.

Although many factors contribute to inaccuracies in kinematic measurements made from single-plane fluoroscopy, this study was limited to a subset of factors. Only one pixel size and grid were selected to represent experimental conditions. Smaller pixels with a higher resolution would likely produce more accurate results. Principle distance between the bone models and the image detector was representative of experimental conditions (1100 mm). As the principle distance decreases, the sensitivity to out-of-plane translation increases. However, if the principal distance becomes too small, shaft geometry from the femur and tibia/fibula is no longer visible in the image, reducing the

sensitivity in other directions. Another factor that influences accuracy is the number of pixels selected for the bone model edges since a larger number of points theoretically will allow more accurate matching. The maximum number of pixels that could be selected was used in this study. Although bone model surface creation could introduce inaccuracies when matching *in vivo* fluoroscopic images, this did not affect the present results since the images were created directly from the bone models used for matching. Assessment of the accuracy of bone model surface geometry created from CT or MRI data (e.g., by comparison with laser scan data) would be valuable in quantifying this potential source of error. Other factors that influenced errors were the higher edge quality in the synthetic images compared to *in vivo* images as well as the omission of interior bone geometry from the analysis.

Evidence suggests that pixel size may determine the minimum errors for single-plane fluoroscopy if bone edge attenuation were not an issue. In our study, the virtual fluoroscope was positioned so that the images had a resolution of 512 x 512 pixels covering a region of 200 x 200 mm. An edge displayed on the pixel grid would lie between two pixels, producing a minimum error of half a pixel, or in our set up about 0.2 mm. The in-plane translation precision for the flat-shaded, randomly-transformed femur and tibia/fibula was between 0.13 and 0.20 mm (Table 1). For the perspective used in our synthetic images, shifting the bone model edges by half a pixel would require approximately 2 mm of translation in the *z* direction. The out-of-plane translation precision for the flat-shaded femur and tibia/fibula was 2.3 to 3.1 mm (Table 1). Thus, increasing the image resolution should have a predictable effect on absolute precision for flat-shaded images with appreciable geometric features.

Matching bone models to single-plane fluoroscopy of the knee requires user intervention to determine the geometry in areas of bone overlaps. For example, the tibia intercondyloid eminence is inserted between the two femural condyles. Therefore, since the outline is not clear, this area is not included in the point cloud defining the bone model image outline. However, this area of the tibia contains the most curvature. This results in a decrease in precision for the tibia/fibula as seen in the synthetic experimental ray-traced sequence. This same effect is not seen in the synthetic random ray-traced sequence, because images for this set were generated using one bone model per image.

Additional bone geometry could be used for matching by detecting bone model inner contours with ray-tracing methods [23]. Since cortical bone attenuates x-rays much more than does cancellous bone (Fig. 3a), ray tracing of bone models produces internal edges that would approximately double the matchable geometry [23]. However, ray tracing is much more costly computationally than is edge detection, which is why ray tracing was not used for bone model edge detection in this study. The extent to which ray tracing would increase matchable geometry and decrease bias is not known, especially given the accuracy limitations imposed by pixel size.

LIST OF REFERENCES

1. Centers for Disease Control and Prevention, Targeting Arthritis: The Nation's Leading Cause of Disability, 2002, National Center for Chronic Disease Prevention and Health Promotion, Atlanta, Georgia.

2. National Hospital Discharge Survey, National Center for Health Statistics, 2003, Hyattsville, Maryland.

3. Hasler, E. M., Herzog, W., Leonard, T. R., Stano, A., and Nguyen, H., 1998, "In vivo knee joint loading and kinematics before and after ACL transection in an animal model," *Journal of Biomechanics*, (31), pp. 253-62.

4. Tashman, S., Anderst, W., and Kolowich, P., 1999, "Severity of OA related to magnitude of dynamic instability in ACL-deficient dogs," In *Transactions of the 46th Annual Meeting of the Orthopaedic Research Society*, Orlando, pp. 257.

5. Kadaba, M. P., Ramakrishnan, H. K., and Wootten, M. E., 1990, "Measurement of lower extremity kinematics during level walking," *Journal of Orthopaedic Research*, (8), pp. 383–92.

6. Lu, L. W., and O'Connor, J. J., 1999, "Bone position estimation from skin marker coordinates using global optimization with joint constraints," *Journal of Biomechanics*, (32), pp. 129–34.

7. Capozzo, A., 1991, "Three-dimensional analysis of human walking: experimental methods and associated artifacts," *Human Movement Science*, (10), pp. 589–602.

8. Lucchitti, L., Cappozzo, A., Cappello, A., and Croce, U. D., 1998, "Skin movement artifact assessment and compensation in the estimation of knee joint kinematics," *Journal of Biomechanics*, (31), pp. 977–84.

9. Pain, M. T. G., and Challis, J. H., 1998, "Measurement of the soft tissue motion of the thigh during an impact," *Presented at the North American Congress of Biomechanics*, Waterloo, ON, Canada.

10. Fuller, J., Liu, L. J., Murphy, M. C., and Mann, R. W., 1997, "A comparison of lower-extremity skeletal kinematics measured using skin- and pin-mounted markers," *Human Movement Science*, (16), pp. 219–42.

11. Spoor, C. W., and Veldpaus, F. E., 1980 "Rigid Body Motion Calculated from spatial coordinates of markers," *Journal of Biomechanics*, (13) pp. 391-3

12. Andriacchi, T. P., Alexander E. J., Toney M. K., Dyrby C. O., and Sum J., 1998, "A point cluster method for in vivo motion analysis: Applied to a study of knee kinematics," *Journal of Biomechanics*, (120), pp. 743-9.

13. Cappozzo, A., Capello, A., Croce, U. D., and Pensalfini, F., 1997, "Surface marker cluster design criteria for 3-D bone movement reconstruction," *IEEE Translactions on Bio-medical Engineering*, (44), pp. 1165-74.

14. Alexander, E. J., and Andriacchi, T. P., 2001, "Correcting for Deformation in Skin-Based Marker Systems," *Journal of Biomechanics*, (34), pp. 355-62.

15. Kaptein, B. L., Valstar, E. R., and Stoel, B. C., 2003, "A new model-based RSA method validated using CAD models and models from reversed engineering," *Journal of Biomechanics*, 36(6), pp 873-82.

16. Zollei, L., Grimson, E., Norbash, A, and Wells, W., 2003, "2D-3D Rigid registration of x-ray fluoroscopy and CT images using mutual information and sparsely sampled histogram estimators," *Artificial Intelligence Laboratory*, MIT, MA, 2003.

17. Banks, S. A., and Hodge, W. A., 1996, "Accurate measurement of three-dimensional knee replacement kinematics using single-plane fluoroscopy," *IEEE Transactions on Bio-medical Engineering*, (43), pp. 638-49.

18. Hoff, W. A., Komistek, R. D., and Dennis, D. A., 1998, "Three-dimensional determination of femoral-tibial contact positions under in vivo conditions using fluoroscopy," *Clinical Biomechanics*, (13), pp. 455-72.

19. Sarojak, M., Hoff, W., Komistek, R., and Dennis, D., 1999 "Interactive system for kinematic analysis of artificial joint implants," *Biomedical Science Instrumentation*, (35), pp. 9-14.

20. Asano, T., Akago, M., Tanaka, K., Tamura, J., and Nakamura, T., 2001, "*In vivo* three-dimensional knee kinematics using a biplanar image-matching technique," *Clinical Orthopaedics and Related Research*, (388), pp. 157-66.

21. Tashman, S., and Anderst, W., 2003, "In vivo measurement of dynamic joint motion using high speed biplane radiography and CT: application to canine ACL deficiency," *Journal of Biomechanical Engineering*, (125), 238-45.

22. You, B., Siy, P., Anderst, W., and Tashman, S., 2001, "In vivo Measurement of 3-D skeletal kinematics from sequences of biplane radiographs: application to knee kinematics," *IEEE Transactions on Medical Imaging*, Jun (20), pp. 514-25.

23. Komistek, R. D., Dennis, D. A., and Mahfouz, M., 2003, "In vivo fluoroscopic analysis of the normal human knee," *Clinical Orthopaedics and Related Research*, (410), pp. 69-81.

24. Kanisawa, I., Banks, A. Z., and Banks, S. A., 2003, "Weight-bearing knee kinematics in subjects with two types of anterior cruciate ligament reconstructions," *Knee Surgery, Sports Traumatology, Arthroscopy*, (11), pp. 16-22.

25. De Guise, J A. and Martel, Y., 1988, "3D biomedical modeling merging image processing and computer aided design," *Proceeding of the Annual International Conference of the IEEE Engineering in Medicine and Biology Society*, New Orleasn, pp. 426-7.

26. Lorensen, W. E., and Cline, H. E., 1987, "Marching cubes: a high resolution 3D surface," *Journal of Computational and Graphical Statistics*, 21(4), pp. 163-9.

27. MacWilliams, B. A., DesJardins, J. D., Wilson, D. R., Romero, J., and Chao, E. Y. S., 1998, "A repeatable alignment method and local coordinate system description for knee joint testing and kinematic measurement," *Journal of Biomechanics,* (31), pp. 947-50.

28. Grood, E. S., and Suntay, W. J., 1983, "A joint coordinate system for the clinical description of three-dimensional motions: application to the knee," *Journal of Biomechanical Engineering*, 105(2), pp. 136-44.

29. Banks, S. A., Markovich, G. D., and Hodge, W.A., 1997, "In vivo kinematics of cruciate-retaining and -substituting knee arthroplasties," *Journal of Arthroplasty*, (12), pp. 297-304.

BIOGRAPHICAL SKETCH

Haseeb A. Rahman received the B.Sc. degree in engineering sciences with a concentration in biomechanics from University of Florida, Gainesville, FL. He has received the Dean's List award 5 times. Mr. Rahman is a member of the National Society of Collegiate Scholars. Mr. Rahman is planning on attending medical school at the University of South Alabama in Mobile, Alabama.

.